Journal of Power Sources 211 (2012) 202–207

Contents lists available at SciVerse ScienceDirect

Journal of Power Sources

journal homepage: www.elsevier.com/locate/jpowsour

Characteristics and electrochemical performance of $LiFe_{0.5}Mn_{0.5}PO_4/C$ used as cathode for aqueous rechargeable lithium battery

Mingshu Zhao*[,1], Guanliang Huang, Bao Zhang, Fei Wang, Xiaoping Song

MOE Key Laboratory for Nonequilibrium Synthesis and Modulation of Condensed Matter, School of Science, Xi'an Jiaotong University, Xi'an 710049, China

ARTICLE INFO

Article history:
Received 8 November 2011
Received in revised form
21 March 2012
Accepted 28 March 2012
Available online 13 April 2012

Keywords:
Lithium ferrous manganese phosphate
Aqueous rechargeable lithium battery
Electrochemical performance
Lithium-ion diffusion efficient

ABSTRACT

$LiFe_{0.5}Mn_{0.5}PO_4/C$ cathode materials are synthesized by a sol–gel method and the precursor calcinations. The phase structures and morphologies are characterized by X-ray diffraction (XRD), transmission electron microscopy (TEM) and high-resolution transmission electron microscopy (HRTEM). Galvanostatic charging/discharging cycles of as-prepared $LiFe_{0.5}Mn_{0.5}PO_4/C$ are performed in the saturated $LiNO_3$ aqueous solution. The initial discharge capacities of ($LiFe_{0.5}Mn_{0.5}PO_4/C$)//LiV_3O_8 aqueous rechargeable lithium battery are 123.09 mAh g^{-1} and 107.00 mAh g^{-1} at 0.05 C and 0.1 C, respectively. And it delivers a capacity of 66.77 mAh g^{-1} at 50 C which is greater than that of 20 C and 30 C, exhibiting good cycling performance at 50 C. This is the first report of a successful utilization of $LiFe_{0.5}Mn_{0.5}PO_4/C$ as cathode material for ARLB and the lithium-ion diffusion coefficients of the $LiFe_{0.5}Mn_{0.5}PO_4/C$ are calculated from the cyclic voltammetry data.

1. Introduction

Lithium-ion batteries have been widely used in the electronic consumable devices, electric vehicles and large-scale energy storage. While they are generally assembled with organic electrolyte, they still cannot meet high power instruments due to safety issue arising from the volatile and flammable organic electrolytes. Therefore, it is of importance to explore new energy storage to improve their safety.

Aqueous rechargeable lithium battery (ARLB) was first put forward by Dahn et al. [1] which consists of $LiMn_2O_4$ cathode and VO_2 anode in 5 M $LiNO_3$ aqueous electrolyte. In comparison to the traditional lithium-ion battery with organic electrolytes, ARLB has several potential advantages such as greater safety and lower cost. Moreover, the ionic conductivity of aqueous electrolyte is much greater than that of the organic electrolyte, which could enable the ARLB to be applied at higher cycling rate with lower electrolyte resistance. Consequently, some cathode materials were used for the ARLB, including $LiMn_2O_4$ [2–5], $LiCoO_2$ [6–8], $LiNiO_2$ [9,10], MnO_2 [11–14], and $LiTi_2(PO_4)_3$ [15,16]. In recent years, much attention has focused on lithium orthophosphates used as the cathode of ARLB due to their high energy density and chemical stability. For $LiFePO_4$, Mi et al. [17] investigated the deintercalation/intercalation behaviors and calculated the corresponding lithium-ion diffusion coefficient of $LiFePO_4$. Xia's group [18] reported (−) $LiTi_2(PO_4)_3|Li_2SO_4|LiFePO_4$(+) ARLB exhibited better capacity retention by eliminating oxygen in the aqueous electrolyte and investigated the mechanism of lithium-ion intercalation in the aqueous electrolyte [19]. The latest literature [20] about modified $LiMnPO_4$ prepared with TiS_2 additive showed that the first discharge capacity in LiOH electrolyte is 90 mAh g^{-1} and its cycling performance was poor at 0.5 mA cm^{-2}. Thus, it is crucial to improve the electrochemical performance of $LiMnPO_4$ in the aqueous electrolyte.

As well known, $LiMnPO_4$ is an insulator with ca. 2 eV energy band gap [21] and the Jahn–Teller effect will cause the interface mismatch of lithiated phase and delithiated phase, which lead to its low electronic conductivity ($<10^{-10}$ S cm^{-1}) [22]. In order to improve its poor electrochemical performance originating from the low electronic conductivity, different approaches have been made by synthesizing nano-sized particles [23–25] and coating carbon [26,27] or doping metal cation to form multi-transition metal olivine compounds [28–32]. Of course, there have been many literatures on the performance of multi-transition metal compounds [28,33–36] in the organic electrolyte, but the electrochemical performances of these compounds used for the ARLB have attracted only little attention. Xia's group [37] reported $LiCo_{1/3}Ni_{1/3}Mn_{1/3}O_2$ combined with activate carbon showed good cycle ability and high rate capability. Zheng [7] pointed out that $LiNi_{1/3}Co_{1/3}Mn_{1/3}O_2$ had a better rate capability and only 9.1% capacity loss after 1000 cycles at 80 C in 2 M $LiNO_3$ solution.

* Corresponding author. Tel.: +86 029 82663034; fax: +86 029 82667872.
E-mail address: zhaomshu@mail.xjtu.edu.cn (M. Zhao).
[1] ISE (International Society of Electrochemistry) member.

0378-7753/$ – see front matter © 2012 Elsevier B.V. All rights reserved.
doi:10.1016/j.jpowsour.2012.03.049

Minakshi [38] studied the crystal structure and phase transition of $Li(Co_{0.5}Ni_{0.5})PO_4$ in an aqueous solution.

In this paper, $LiFe_{0.5}Mn_{0.5}PO_4/C$ compounds were prepared by a sol–gel method and sintering process. The ARLB was assembled with $LiFe_{0.5}Mn_{0.5}PO_4/C$ and LiV_3O_8 in saturated $LiNO_3$ solution. The galvanostatic charging/discharging experiments were used to evaluate the electrochemical behaviors of $LiFe_{0.5}Mn_{0.5}PO_4/C$ and the lithium-ion diffusion coefficients of $LiFe_{0.5}Mn_{0.5}PO_4/C$ were studied with CV data.

2. Experimental

$LiFe_{0.5}Mn_{0.5}PO_4/C$ was synthesized by a sol–gel and calcinations process. $CH_3COOLi\cdot 2H_2O$, $FeCl_2\cdot 4H_2O$, $MnCl_2\cdot 4H_2O$, P_2O_5 and critic acid with a molar ratio of 1:0.5:0.5:1:1 were dissolved in 40 mL ethanol solution. The mixture solution was rigorous stirred for 12 h in nitrogen gas, and then heated at 353 K to get xerogel. Finally, the xerogel was fired at 773 K for 5 h in the purified argon gas flowing to prevent the oxidation of Fe^{2+} to obtain $LiFe_{0.5}Mn_{0.5}PO_4/C$. LiV_3O_8 was synthesized as describe as previous publication [5].

The three-electrode cell was constructed with the $LiFe_{0.5}Mn_{0.5}PO_4/C$ cathode (15 mm in length, 5 mm in width, 0.2 mm in thickness, and active material weighing 12 mg) as the working electrode, LiV_3O_8 anode (with identical dimensions to the cathode) as counter electrode, and saturate calomel electrode (0.242 vs. SHE/V) as reference electrode. The working electrode was prepared as following: mixing active materials ($LiFe_{0.5}Mn_{0.5}PO_4/C$), acetylene black and polyvinylidene fluoride(PVDF) in a weight ratio of 80:10:10 using N-methyl-2-pyrrolidone as solvent, the black slurry was uniform mixed with ultrasonic process for 2 min, then coated on nickel mesh followed by drying at 373 K for 10 h under vacuum. The counter electrode was prepared by the same method as the working electrode described above. The relative ratio of cathode and anode amounts is 1:1.2. The neutral electrolyte was prepared by dissolving appropriate amount of $LiOH\cdot H_2O$ in the saturated $LiNO_3$ solution, and the experimental deoxygenated electrolyte was

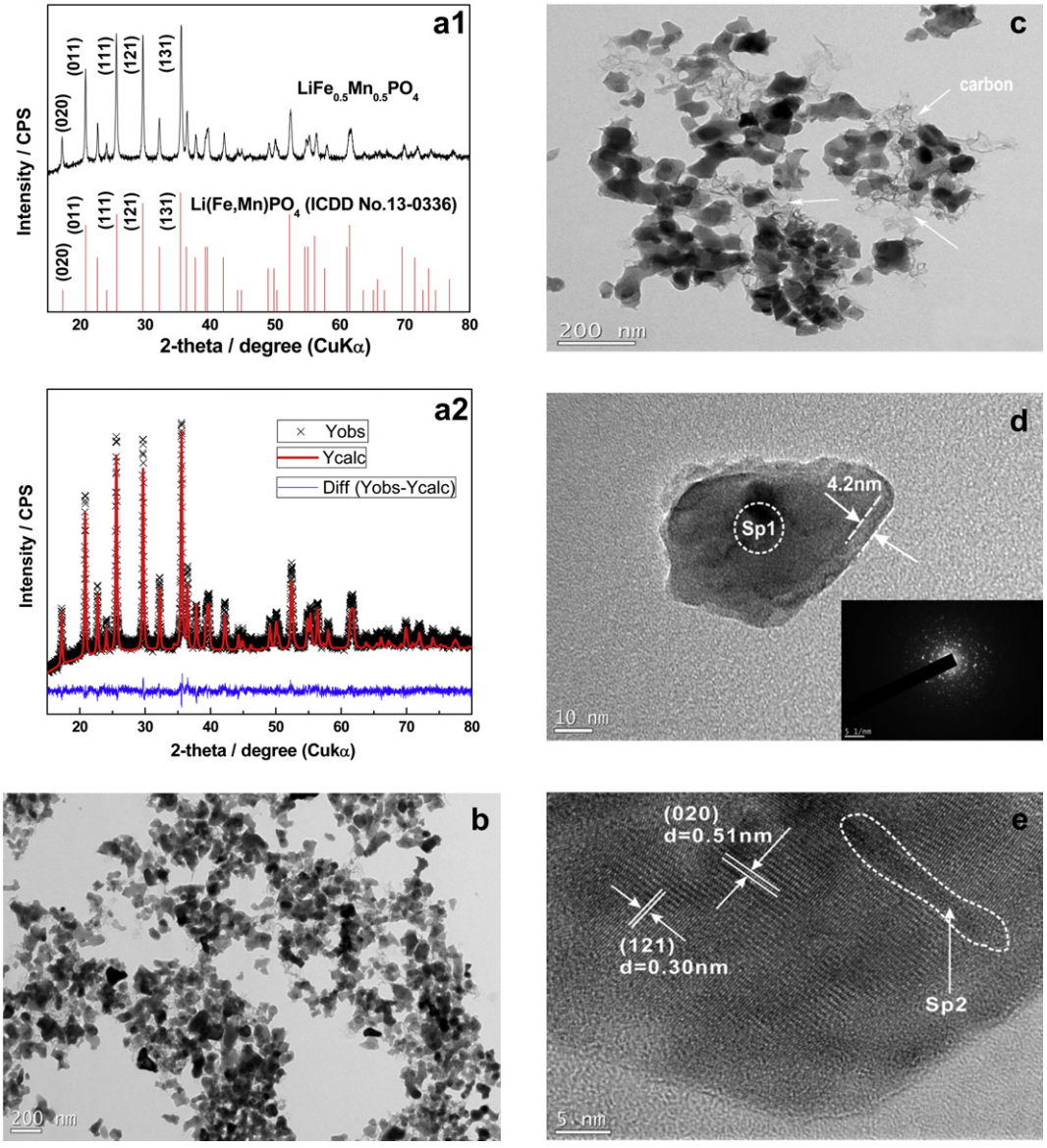

Fig. 1. (a1) XRD pattern comparison between the $LiFe_{0.5}Mn_{0.5}PO_4/C$ and ICDD No. 13-0336. (a2) The Rietveld refinement result of $LiFe_{0.5}Mn_{0.5}PO_4/C$. (b–d) TEM images and (e) HRTEM images of $LiFe_{0.5}Mn_{0.5}PO_4/C$.

prepared by bubbling high-purity nitrogen for 3 h before measurement.

The sample was characterized by XRD analysis using Bruker D8-Adavanced diffractometer with Cu Kα radiation, scanning ranges from 15° to 80°. The lattice parameters of the as-synthesized sample are refined by Rietveld analysis using the Topas software. The actual electrode surface area was measured with BET method by using ASAP 2020. The element analysis of the precipitation in the aqueous electrolyte was studied by a JEOL JSM-7000F instrument and an energy dispersive X-ray (EDS) spectrometer. The micro-morphologies of the as-prepared materials were observed using JEOL JEM-2100 transmission electron microscope operating at an accelerating voltage of 200 kV. The electrochemical properties were performed using Arbin BT2000 instrument controlled by Arbin MITS PRO. Cyclic voltammetric experiments were recorded at the scanning rate of 0.1 mV s^{-1}, 1 mV s^{-1}, 2 mV s^{-1}, 2.5 mV s^{-1}, 4 mV s^{-1} and 10 mV s^{-1} within the potential range of −0.4 V to 1.2 V vs. SCE using AMETEK VMC-4. All the measurements were conducted at room temperature.

3. Result and discussion

The XRD pattern of $LiFe_{0.5}Mn_{0.5}PO_4/C$ is shown in Fig. 1a1. The crystal structure of the sample is consistent with standard ordered olivine structure of ICDD No. 13-0336. In the standard XRD pattern of $LiFe_{0.5}Mn_{0.5}PO_4$, the peak intensity ratios of (111) and (121), (121) and (131) are 0.89, 0.90, respectively. Nevertheless, the peak intensity ratios of the synthesized $LiFe_{0.5}Mn_{0.5}PO_4/C$ are 1.01 and 0.97. These changes in peak intensity ratios are mainly due to a little distortion of the crystal lattice of $LiMnPO_4$ caused by Fe atoms. Compared with pure $LiMnPO_4$ (ICSD No. 97763: $a = 10.431$ Å, $b = 6.095$ Å, $c = 4.734$ Å), using the Rietveld refinement method, the calculated lattice parameters are $a = 10.387$ Å, $b = 6.052$ Å and $c = 4.720$ Å, and $R_{wp} = 1.25$, $R_p = 0.99$. The refinement result of

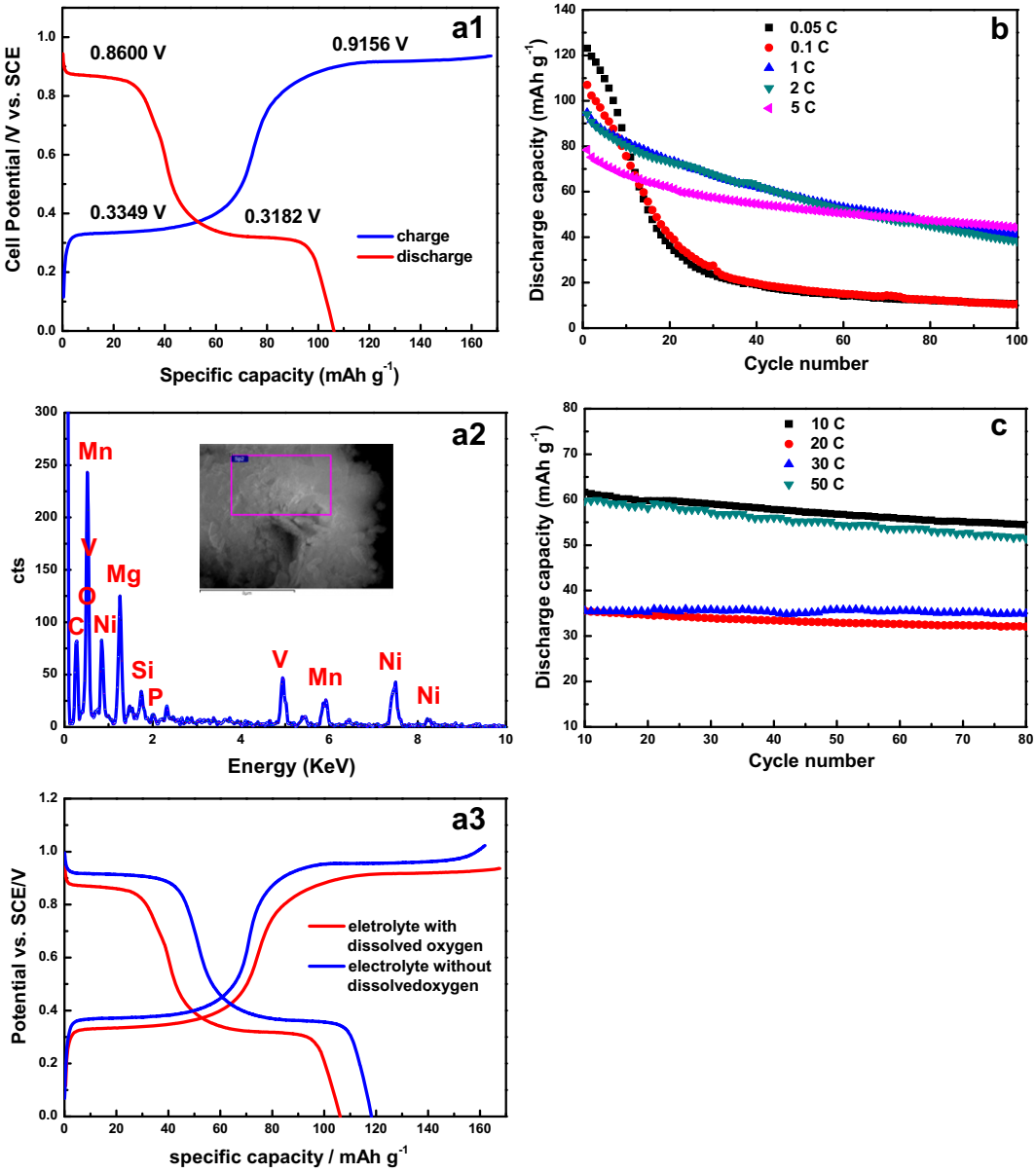

Fig. 2. Electrochemical performance of $(LiFe_{0.5}Mn_{0.5}PO_4/C)//LiV_3O_8$ for ARLB. (a1) The initial charge–discharge curves at 0.1 C. (a2) The EDS of the precipitation in the electrolyte. (a3) The galvanostatic charge–discharge curves of $LiFe_{0.5}Mn_{0.5}PO_4/C$ at 0.1 C in $LiNO_3$ electrolyte with or without dissolved oxygen. (b) Cycling behaviors of $(LiFe_{0.5}Mn_{0.5}PO_4/C)//LiV_3O_8$ at different rates of 0.05 C, 0.1 C, 1 C, 2 C and 5 C. (c) Cycling behaviors of $(LiFe_{0.5}Mn_{0.5}PO_4/C)//LiV_3O_8$ at different rates of 10 C, 20 C, 30 C and 50 C.

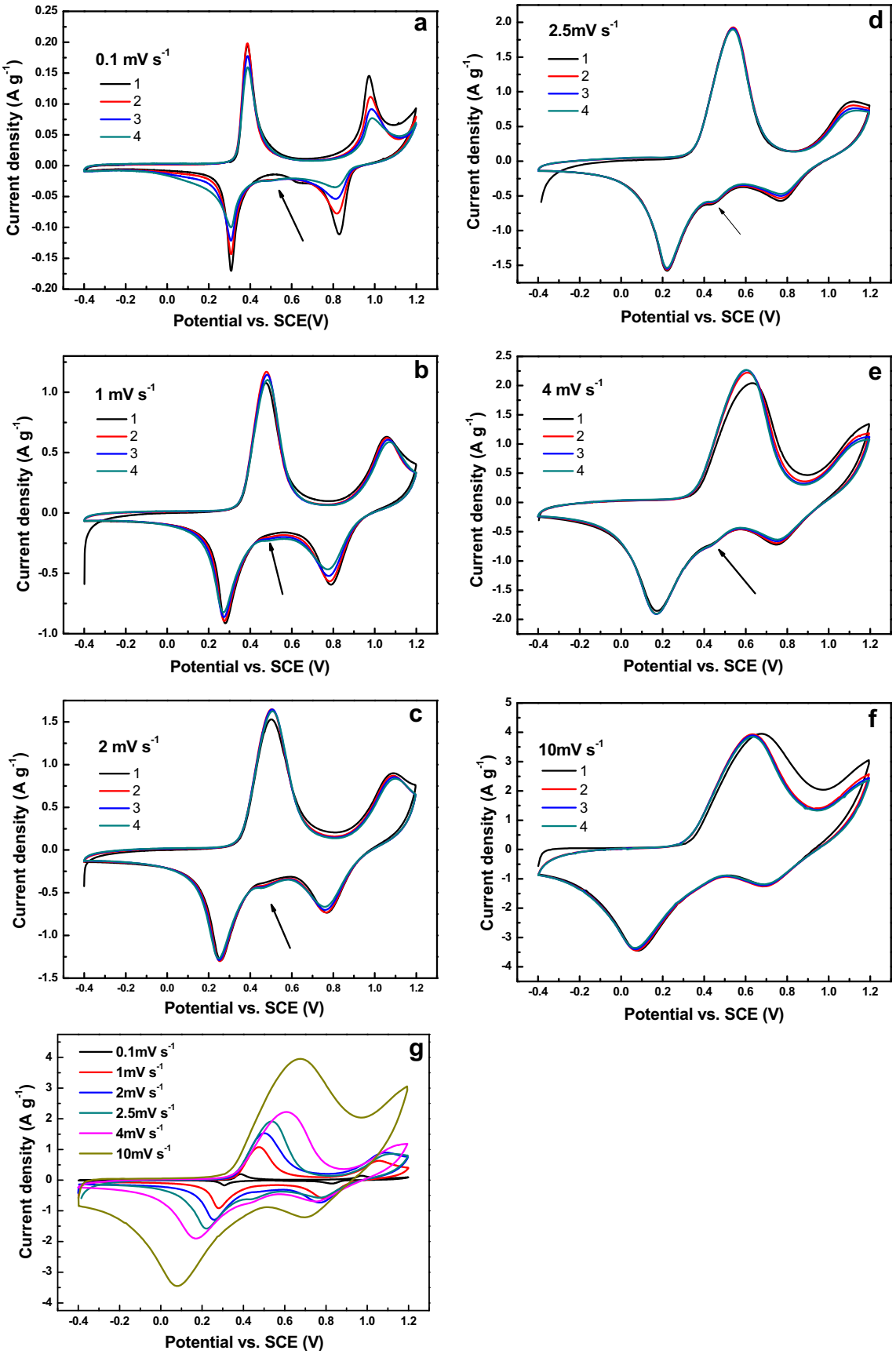

Fig. 3. The cyclic voltammograms of $LiFe_{0.5}Mn_{0.5}PO_4/C$ in saturated $LiNO_3$ aqueous electrolyte at different scanning rates. (a) 0.1 mV s^{-1}, (b) 1 mV s^{-1}, (c) 2 mV s^{-1}, (d) 2.5 mV s^{-1}, (e) 4 mV s^{-1}, (f) 10 mV s^{-1}, (g) comparison of the initial cycle of $LiFe_{0.5}Mn_{0.5}PO_4/C$ at 0.1 mV s^{-1}, 1 mV s^{-1}, 2 mV s^{-1}, 2.5 mV s^{-1}, 4 mV s^{-1} and 10 mV s^{-1}.

$LiFe_{0.5}Mn_{0.5}PO_4/C$ is presented in Fig. 1a2, which suggests that Fe atoms cause the decrease of the lattice parameters.

The TEM and HRTEM images of as-prepared materials were shown in Fig. 1b–f. In Fig. 1b, the particles are dispersed uniformly and their sizes range from 50 nm to 200 nm. In Fig. 1c, the dispersed particles are connected with the numerous and continuous carbon substance marked with white arrows. The critic acid was decomposed to carbon during the sintering process, and it appeared not only in the layer form but also in the granular form separated for the olivine particles. In Fig. 1d, the carbon layer is about 4.2 nm thickness. The carbon coating amount is 9.7 wt% in $LiFe_{0.5}Mn_{0.5}PO_4/C$. The insert image of Fig. 1d is the electron diffusion pattern of the marked "Sp1", exhibiting that the particle is composed of many smaller crystallite. Fig. 1e illustrates the HRTEM images of $LiFe_{0.5}Mn_{0.5}PO_4/C$. The spacing of lattice fringes are 0.51 nm, 0.30 nm and 0.43 nm, corresponding to (020) and (121) plane of $LiFe_{0.5}Mn_{0.5}PO_4/C$. These results indicate that $LiFe_{0.5}Mn_{0.5}PO_4/C$ is well crystallized, meanwhile, it has some crystal defects observed from the region marked with "Sp2".

The 1st charge–discharge curve of $LiFe_{0.5}Mn_{0.5}PO_4/C$ at 0.1 C is shown in Fig. 2a1. The 1st discharge capacity is 107.00 mAh g^{-1}, which is higher than that reported in Ref. [35]. In Fig. 2a1, two pairs of voltage plateaus are observed, related to the charge/discharge reactions of Fe^{2+}/Fe^{3+} (charge: 0.3349 V; discharge: 0.3182 V) and Mn^{2+}/Mn^{3+} (charge: 0.9156 V; discharge: 0.8600 V) with polarization potential of 0.0167 V and 0.0556 V, respectively. The reduced polarization potential 0.0556 V of Mn redox couple is much lower than that of the reported in the recent paper [20]. However, the coulombic efficiency of this ARLB is relatively low, which may be attributed to Jahn–Teller effect, manganese dissolution or the dissolved oxygen in the aqueous electrolyte. As shown in Fig. 2a2, the corresponding EDS spectra of the precipitation in the aqueous electrolyte after the first cycle, exhibit characteristics peaks of manganese, and the formation of precipitation we proposed is shown as following reaction: $2Mn^{2+}{}_{(dissolution)} + 2H_2O + O_2 + 4e^- = 2Mn(OH)_2\downarrow$. In Fig. 2a3, the comparisons of 1st charge–discharge curves for $LiFe_{0.5}Mn_{0.5}PO_4/C$ in dissolved oxygen $LiNO_3$ aqueous electrolyte and in $LiNO_3$ aqueous electrolyte without dissolved oxygen indicate that the coulombic efficiency and discharge capacity could be improved by eliminating oxygen in the aqueous electrolyte.

The electrochemical cycle behaviors of $(LiFe_{0.5}Mn_{0.5}PO_4/C)//LiV_3O_8$ ARLB at different C-rate are shown in Fig. 2b. The initial discharge capacity of ARLB at 0.05 C, 0.1 C, 1 C, 2 C, 5 C are 123.09 mAh g^{-1}, 107.00 mAh g^{-1}, 94.75 mAh g^{-1}, 94.07 mAh g^{-1}, 78.39 mAh g^{-1}, respectively. However, the fast capacity fade is observed and the retained discharge capacities are only 10.65 mAh g^{-1}, 10.42 mAh g^{-1}, 40.73 mAh g^{-1}, 38.21 mAh g^{-1}, 44.25 mAh g^{-1} after 100 cycles. Fig. 2c illustrates the cycle performance of $(LiFe_{0.5}Mn_{0.5}PO_4/C)//LiV_3O_8$ ARLB at different higher C-rate. As shown in Fig. 2c, the 1st discharge capacity of 68.37 mAh g^{-1}, 37.36 mAh g^{-1}, 34.62 mAh g^{-1} and 66.77 mAh g^{-1} could still be obtained at the rate of 10 C, 20 C, 30 C and 50 C, respectively. The discharge capacity is still above 50 mAh g^{-1} after 100 cycles at 50 C, and it is the first report of $(LiFe_{0.5}Mn_{0.5}PO_4/C)//LiV_3O_8$ ARLB at 50 C. It is noted that the discharge capacity at 50 C is higher than that at 20 C and 30 C in our experiment; and this unusual phenomena in the ARLB is also reported in [5,39], which is quite different from the traditional lithium-ion battery. The reason should be studied intensively.

The cyclic voltammogram curves of $LiFe_{0.5}Mn_{0.5}PO_4/C$ electrodes in saturated $LiNO_3$ electrolyte at different scanning rate are shown in Fig. 3a–f. Two pairs of redox peaks, which are associated with the lithium-ion deintercalation/intercalation in the process of the oxidation/reduction of Fe^{2+}/Fe^{3+} and Mn^{2+}/Mn^{3+}, appear in the CV curves at scanning rate of 0.1 mV s^{-1}, 1.0 mV s^{-1}, 2 mV s^{-1}, 2.5 mV s^{-1}. Nevertheless, at the scanning rate of 4.0 mV s^{-1} and 10 mV s^{-1}, the Mn anodic peak of the CV curve for $LiFe_{0.5}Mn_{0.5}PO_4/C$ is not found due to the potential moves positively exceeding the measurement range (from −0.4 V to 1.2 V). At the scanning rate of 0.1 mV s^{-1}, 1.0 mV s^{-1}, 2 mV s^{-1}, the peak potentials do not change and the peak currents decline largely with the increase of the cycle number. On the contrary, for the 2.5 mV s^{-1}, 4 mV s^{-1} and 10 mV s^{-1}, though the oxidation peaks shift slightly lower potential in the second cycle and there are some irreversible capacity loss, the CV curves appear well-defined peaks and good overlap in the following cycles. The above results illustrate that $LiFe_{0.5}Mn_{0.5}PO_4/C$ has good cycle ability in the ARLB at high scanning rate. Moreover, the additional peaks indicate by the dark arrows, which locate between 0.2 V and 0.8 V, are found in the CV profiles. We presume that the additional peak may be associated with the intrinsic structure, the proton insertion [7] or the reaction of impurities existing in the aqueous electrolyte.

In order to compare CV curves of $LiFe_{0.5}Mn_{0.5}PO_4/C$ at different scanning rate, we displayed them in Fig. 3g. Table 1 listed the peak potential difference ($E_{p,a} - E_{p,c}$) at various scanning rates calculated from Fig. 3g for $LiFe_{0.5}Mn_{0.5}PO_4/C$. According to the CV curves, we could evaluate the reaction reversibility, and that is the peak potential difference ($E_{p,a} - E_{p,c}$). The results indicate that the peak currents and the peak potential difference between the anodic and cathodic peaks of Fe and Mn increase with the scanning rate increasing. The ARLB may yield quasi-reversible waves at 0.1 mV s^{-1} and 1 mV s^{-1}, however, irreversible behaviors are observed at 2 mV s^{-1}, 2.5 mV s^{-1}, 4 mV s^{-1} and 10 mV s^{-1}, which may be assumed that the electrochemical lithium-ion deintercalation/intercalation process changes from being kinetically quasi-reversible to irreversible when scanning rate increases from being low to high.

Fig. 4 shows the linear relationship between the peak currents and the square root of the scanning rate for the anodic and cathodic process. It appears that the lithium-ion deintercalation/intercalation process is diffusion-controlled for $LiFe_{0.5}Mn_{0.5}PO_4/C$ used in the ARLB, which is in accordance with Ref. [40]. And then, the diffusion coefficients of lithium ion for $LiFe_{0.5}Mn_{0.5}PO_4/C$ can be roughly calculated according to the Eq.(1) [41]

$$i_p = 0.4463\left(\frac{F^3}{RT}\right)^{1/2} n^{3/2} A D^{1/2} C_0^* \nu^{1/2} \quad (1)$$

where i_p is peak current, F is Faraday's constant, R is the gas constant, T is the absolute temperature, n is electrons per molecule lithium ion, $\nu^{1/2}$ is scanning rate of cyclic voltammetry, C_0^* is concentration of lithium ion, A is the actual surface area of electrode and its value calculated by BET method is 1747 cm^{-2}, D is the diffusion efficient of lithium ion. The corresponding diffusion coefficients are list in Table 2. In Table 2, the magnitude order of lithium-ion diffusion coefficient from $D_{Fe(anodic)/(cathodic)}$ is 10^{-14} cm^2 S^{-1}, which is lower than that reported in Ref. [17]; while $D_{Mn(anodic)/(cathodic)}$ is about 10^{-14}–10^{-15} cm^2 S^{-1}, which is higher than that reported in Ref. [42]. In terms of the lithium-ion

Table 1
Peak potential difference ($E_{p,a} - E_{p,c}$) at various scan rates calculated from Fig. 3g for $LiFe_{0.5}Mn_{0.5}PO_4/C$.

Scan rate/mV s^{-1}	($E_{p,a} - E_{p,c}$) for Fe/mV	($E_{p,a} - E_{p,c}$) for Mn/mV
0.1	79	154
1	200	273
2	271	323
2.5	326	402
4	443	–
10	557	–

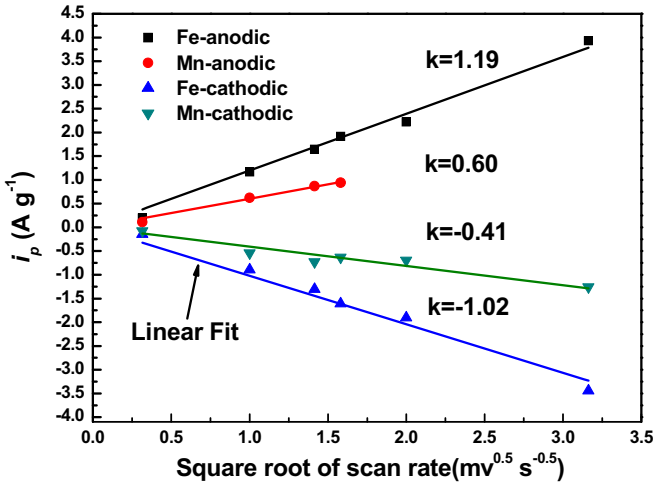

Fig. 4. The relationship between the peak currents and the square root of the scanning rate of $LiFe_{0.5}Mn_{0.5}PO_4/C$.

Table 2
Lithium-ion diffusion coefficient calculated from Fig. 4 for $LiFe_{0.5}Mn_{0.5}PO_4/C$.

Material	$D_{Fe(anodic)}$/ $cm^2\,S^{-1}$	$D_{Mn(anodic)}$/ $cm^2\,S^{-1}$	$D_{Fe(cathodic)}$/ $cm^2\,S^{-1}$	$D_{Mn(cathodic)}$/ $cm^2\,S^{-1}$
$LiFe_{0.5}Mn_{0.5}PO_4$	7.13×10^{-14}	1.81×10^{-14}	5.24×10^{-14}	8.46×10^{-15}

coefficient of $LiFe_{0.5}Mn_{0.5}PO_4/C$ used for the ARLB, further studies are still required.

4. Conclusion

The electrochemical performances of new intercalate electrode material, $LiFe_{0.5}Mn_{0.5}PO_4/C$, in saturated $LiNO_3$ aqueous electrolyte are firstly studied by galvanostatic cycling and cyclic voltammetry. The $(LiFe_{0.5}Mn_{0.5}PO_4/C)//LiV_3O_8$ ARLB exhibits good cycling stability at higher C-rate. And it shows great potential for applications in large-scale devices. The detailed cyclic voltammetry investigations show that the lithium-ion deintercalation/intercalation process of $LiFe_{0.5}Mn_{0.5}PO_4/C$ used in the ARLB is diffusion-controlled.

Acknowledgments

The authors acknowledge the Province Natural Science Foundation of Shaan Xi (2010JM6018), Xi'an Science and Technology plan project (CXY1124), and the Fundamental Research Funds for the Central University (0109-08143057).

Appendix A. Supplementary material

Supplementary material associated with this article can be found, in the online version, at doi:10.1016/j.jpowsour.2012.03.049.

References

[1] W. Li, J.R. Dahn, D.S. Wainwright, Science 264 (1994) 1115.
[2] L. Tian, A. Yuan, J. Power Sources 192 (2009) 693.
[3] W. Tang, S. Tian, L.L. Liu, L. Li, H.P. Zhang, Y.B. Yue, Y. Bai, Y.P. Wu, K. Zhu, Electrochem. Commun. 13 (2011) 205.
[4] J.H. Yi, J.H. Kim, H.Y. KooO, Y.N. Ko, J. Power Sources 196 (2011) 2858.
[5] M. Zhao, X. Song, F. Wang, W. Dai, X. Lu, Electrochim. Acta 56 (2011) 5673.
[6] W. Tang, L.L. Liu, S. Tian, L. Li, Y.B. Yue, Y.P. Wu, S.Y. Guan, K. Zhu, Electrochem. Commun. 12 (2010) 1524.
[7] J. Zheng, J.J. Chen, X. Jia, J. Song, C. Wang, M.S. Zheng, Q.F. Dong, J. Electrochem. Soc. 157 (2010) A702.
[8] R. Ruffo, F.L. Mantia, C. Wessells, R.A. Huggins, Y. Cui, Solid State Ionics 192 (2011) 289.
[9] M.M. Rao, M. Jayalakshmi, O. Schäf, U. Guth, H. Wul, F. Scholz, J. Solid State Electrochem. 4 (1999) 17.
[10] X. Lai, D. Gao, J. Bi, Y. Li, P. Cheng, C. Xu, D. Lin, J. Alloys Compd. 487 (2009) L30.
[11] M. Minakshi, P. Singh, D.R.G. Mitchell, J. Electrochem. Soc. 154 (2007) A109.
[12] M.S. Wu, R.H. Lee, J. Power Sources 176 (2008) 363.
[13] M. Minakshi, D.R.G. Mitchell, Electrochim. Acta 53 (2008) 6323.
[14] M. Minakshi, M. Blackford, M. Ionescu, J. Alloys Compd. 509 (2011) 5947.
[15] J.Y. Luo, Y. Yao Xia, Adv. Funct. Mater. 17 (2007) 3877.
[16] J.Y. Luo, Y.Y. Xia, J. Power Sources 186 (2009) 224.
[17] C.H. Mi, X.G. Zhang, H.L. Li, J. Electroanal. Chem. 602 (2007) 245.
[18] J.Y. Luo, W.J. Cui, P. He, Y.Y. Xia, Nat. Chem. 2 (2010) 760.
[19] P. He, J.L. Liu, W.J. Cui, J.Y. Luo, Y.Y. Xia, Electrochim. Acta 56 (2011) 2351.
[20] M. Minakshi, A. Pandey, M. Blackford, M. Ionescu, Energy Fuels 24 (2010) 6193.
[21] A. Yamada, M. Hosoya, S.C. Chung, Y. Kudo, K. Hinokuma, K.Y. Liu, Y. Nishi, J. Power Sources 119–121 (2003) 232.
[22] M. Yonemura, A. Yamada, Y. Takei, N. Sonoyamam, R. Kanno, J. Electrochem. Soc. 151 (2004) A1352.
[23] D. Choi, D.H. Wang, I. Bae, J. Xiao, Z. Nie, W. Wang, V.V. Viswanathan, Y.J. Lee, J.G. Zhang, G.L. Graff, Z.G. Yang, J. Liu, Nano Lett. 10 (2010) 2799.
[24] Z. Bakenov, I. Taniguchi, Electrochem. Commun. 12 (2010) 75.
[25] D. Rangappa, K. Sone, Y. Zhou, T. Kudo, I. Honma, J. Mater. Chem. 21 (2011) 15813.
[26] S.M. Oh, S.W. Oh, C.S. Yoon, B. Scrosati, K. Amine, Y.K. Sun, Adv. Funct. Mater. 20 (2010) 3260.
[27] P.R. Kumar, M. Venkateswarlu, M. Misra, A.K. Mohanty, N. Satyanarayana, J. Electrochem. Soc. 158 (2011) A227.
[28] C. Hu, H. Yi, H. Fang, B. Yang, Y. Yao, W. Ma, Y. Dai, Electrochem. Commun. 12 (2010) 1784.
[29] H. Gwon, D.H. Seo, S.W. Kim, J. Kim, K. Kang, Adv. Funct. Mater. 19 (2009) 3285.
[30] J.W. Leea, M.S. Park, B. Anass, J.H. Park, M.S. Paik, S.G. Doo, Electrochim. Acta 55 (2010) 4162.
[31] G.Y. Chen, A.K. Shukla, X.Y. Song, T.J. Richardson, J. Mater. Chem. 21 (2011) 10126.
[32] H.L. Wang, Y. Yang, Y. Liang, L.F. Cui, H.S. Casalongue, Y. Li, G. Hong, Y. Cui, H. Dai, Angew. Chem. 123 (2011) 7502.
[33] J. Yao, S. Bewlay, K. Konstantionv, V.A. Drozd, R.S. Liu, X.L. Wang, H.K. Liu, G.X. Wang, J. Alloys Compd. 425 (2006) 363.
[34] J. Kim, D.H. Seo, S.W. Kim, Y.U. Park, K. Kang, Chem. Commun. 46 (2010) 1305.
[35] K. Saravanan, J.J. Vittal, M.V. Reddy, B.V.R. Chowdari, P. Balaya, J. Solid State Electrochem. 14 (2010) 1755.
[36] J. Hong, F. Wang, X. Wang, J. Graetz, J. Power Sources 196 (2011) 3659.
[37] Y.G. Wang, J.Y. Luo, C.X. Wang, Y.Y. Xia, J. Electrochem. Soc. 153 (2006) A1425.
[38] M. Minakshi, N. Sharma, D. Ralph, D. Appadoo, K. Nallathamby, Electrochem. Solid-State Lett. 14 (2011) A86.
[39] S. Liu, S.H. Ye, C.Z. Li, G.L. Pan, X.P. Gao, J. Electrochem. Soc. 158 (2011) A1490.
[40] A.J. Bard, L.R. Faulkner, Electrochemical Methods: Fundamentals and Applications, second ed., John Wiley & Sons, New York, 2001.
[41] A.J. Bard, L.R. Feaulkner, Electrochemical Methods, John Wiley & Sons, Inc, New York, 1980.
[42] A.M. Hashambhoy, J.F. Whitacre, J. Electrochem. Soc. 158 (2011) A390.